Simulations of Tetra-Tethered Organic/Inorganic Nanocube−Polymer Assemblies

Elaine R. Chan,[†] Xi Zhang,[‡] Cheng-Ying Lee,[§] Matthew Neurock,[§] and Sharon C. Glotzer*[,†,‡]

Departments of Chemical Engineering and Materials Science & Engineering, University of Michigan, Ann Arbor, Michigan 48109-2136, and Department of Chemical Engineering, University of Virginia, Charlottesville, Virginia 22904-4741

Received November 5, 2004; Revised Manuscript Received April 22, 2005

ABSTRACT: We perform molecular simulations to study the self-assembly of tetratethered nanoparticles with a cubic geometry. We develop a minimal model of the tethered nanoscale building block (NBB) to represent a polyhedral oligomeric silsesquioxane (POSS) molecule with polymeric functionalities based on information about the molecular structure and interactions obtained from ab initio density functional theory calculations. Using this model, we explore the rich nanostructures formed from self-assembly of the NBBs and make analogies with the morphologies observed in block copolymer, surfactant, and liquid crystalline systems. On the basis of the assembled structures produced and determination of the location and nature of the order−disorder transitions in the system, we propose phase diagrams to describe the behavior of these molecules. We find that qualitative similarities exist between the phase diagrams for the tetratethered NBBs and those for block copolymer and surfactant systems.

I. Introduction

Self-assembly offers a promising strategy for manipulating the bottom-up assembly of nanometer-scale objects into useful structures for many diverse applications.[1] Synthetic methods now afford a remarkable variety of nanoscale building blocks (NBBs), and functionalization of these NBBs with synthetic and biological macromolecules provides potential opportunities to control and design the assembly of the building blocks into materials and devices with novel or enhanced properties.

Polyhedral oligomeric silsesquioxane (POSS) molecules are a novel class of building block with immense potential for constructing hybrid organic/inorganic materials with superior physical properties.[2−6] These nanocubes consist of silicon and oxygen atoms linked into a well-defined, cubic inorganic cage with silicon atoms at the corners and oxygen atoms interspersed along the edges. The salient feature of this particular NBB is the ability to functionalize the silicon corners with a variety of organic substituents,[7,8] including block copolymers,[9] olefins and epoxides,[10] mesogenic groups,[11−14] and biological molecules such as peptides[15] and carbohydrates.[16] Materials derived from POSS molecules are expected to demonstrate enhanced properties by bridging the property space between organic substituent and inorganic silsesquioxane materials. The specific functionalities on a POSS molecule can impart unique thermal, mechanical, optical, rheological, solubility, and diffusivity properties to materials, thereby rendering them as potential candidates for a variety of applications such as photonic materials[17] and catalysis.[18]

In the context of self-assembly, POSS chemistry provides a promising means for precisely manipulating the topology and architecture of the NBB to control the assembly of the molecules into specific structures, yielding hybrid materials with tailored properties. For example, experimental studies on liquid crystalline POSS molecules reveal that covalently attaching mesogenic[13] and rigid nonmesomorphic[11] substituents to the silsesquioxane core enables the NBB to form liquid crystalline phases that the substituents themselves do not exhibit and thereby demonstrate that direct attachment of the relatively rigid POSS cubes influences the types of structures formed and increases the variety of self-assembled structures possible.

There are many more experimental demonstrations of the self-assembly of POSS−polymer pendant copolymers[19−23] and polymer-tethered POSS molecules into higher-order micellar and vesicular, lamellar, and cylindrical structures. Of increasing interest are experimental studies on polymer-tethered POSS molecules that illustrate the potential of the building block strategy for generating hybrid organic/inorganic structures. Recently, several groups have investigated the self-assembly of tethered amphiphilic POSS molecules. Knischka et al.[24] synthesized POSS molecules with a single poly(ethylene oxide) (PEO) tether and observed aggregation of the NBBs into micelles and vesicles in aqueous solution. Kim and co-workers[25] investigated the self-assembly of POSS molecules with a polyoxazoline tether attached at one of the cube corners. They found that the NBBs formed spherical micelles in aqueous solution, with the micellar core composed of the hydrophobic cubes and an outer hydrophilic shell composed of tethers. The critical micelle concentration and the size of the micelles were greater than those in conventional amphiphilic block copolymer systems, suggesting that higher concentrations of POSS NBBs are needed to induce micellar formation than those required in systems of block copolymers. They also found that shorter tether lengths suppressed micelle formation, most likely because of poor dispersion of POSS in solution at higher molar ratios. Kim and Mather[26] synthesized amphiphilic

[†] Department of Chemical Engineering, University of Michigan.
[‡] Department of Materials Science & Engineering, University of Michigan.
[§] University of Virginia.
* Corresponding author: E-mail sglotzer@umich.edu.

10.1021/ma047722l CCC: $30.25
Published on Web 06/15/2005

POSS telechelic molecules consisting of two POSS cages that are connected by a poly(ethylene glycol) (PEG) tether in a dumbbell configuration. They discovered that the POSS cubes suppress crystallization of the PEO segments for low molecular weight tethers to yield amorphous morphologies. Interestingly, the telechelic molecules exhibited altered solubility behavior, as they were insoluble in both water and hexane, which are good solvents for PEG homopolymers and cyclohexyl-functionalized POSS cubes, respectively.

Studies of other tethered POSS−polymer systems have been explored as well. Cardoen and Coughlin[27] synthesized hemi-telechelic POSS molecules with a single polystyrene tether in organic solvent. They observed alternating layers of POSS and polystyrene that suggests a lamellar or cylindrical morphology. The aggregate size of the POSS domains was found to decrease as the tether length increases, with the possibility of complete suppression of aggregation for sufficiently long tethers.

In conjunction with these experiments, computer simulations and theory can provide fundamental insight into the self-assembly process and are valuable tools for identifying and efficiently mapping the vast parameter space of complex POSS assemblies and general systems of tethered NBBs in a systematic manner.[28−30] Here we present Brownian dynamics simulations of the self-assembly of tetratethered cubic NBBs, that is, cubes with four tethers attached to one side. For the present work, we regard the tethered NBB as a "minimal" representation of a POSS cube with polymer functionalities, although its applicability to platinum[31] and gold and silver[32] nanocubes, and general systems of cuboids,[33] with tethers on four corners may also be considered. We investigate how the assembly and spatial distribution of the NBBs are affected by the solvent quality, temperature, concentration, and length of the tether functionalities. These results are compared with the self-assembled microstructures observed in block copolymer, surfactant, and liquid crystalline systems to gain insight on the self-assembly behavior of tethered POSS systems. This study demonstrates how our simulation approach is instructive for gaining an understanding of the assembly process and the important parameters governing the fabrication of "shape amphiphiles"—amphiphilic building blocks where the geometry of the various parts of the amphiphile induces novel packing behavior. In a separate paper, we report on the phase behavior of monotethered POSS cubes.[34]

II. Model Development

A. Methodology. We wish to draw upon knowledge of the rich self-assembled morphologies predicted and observed for block copolymers, surfactants, and liquid crystalline molecules as a starting point for studying the self-assembly of tethered POSS into ordered nanostructures. Thus far, there have been reports mainly on the synthesis and characterization of both monofunctionalized POSS molecules $R'R_7Si_8O_{12}$,[35] where seven of the eight Si corners are functionalized with the same substituent and octafunctionalized POSS molecules $R_8Si_8O_{12}$,[4] where all eight Si corners are functionalized with identical substituents. The synthesis and characterization of tetrasubstituted POSS have been reported for liquid crystalline POSS molecules having four Si corners functionalized with hydrogen atoms and the other four Si corners with mesogens.[11,36] Here we propose a novel tetratethered POSS molecule $R'_4R_4Si_8O_{12}$ with four homopolymer tethers R′ each attached to Si atoms that comprise the same face of the cubic cage (Figure 1). R can be considered an atomic or small organic group for simplicity. The symmetrical structure of the tetratethered molecule makes it a better analogue to linear diblock copolymer and surfactant molecules as compared to monofunctionalized POSS molecules that are highly asymmetric due to functionalization of the cage with just one tether (R′ group).

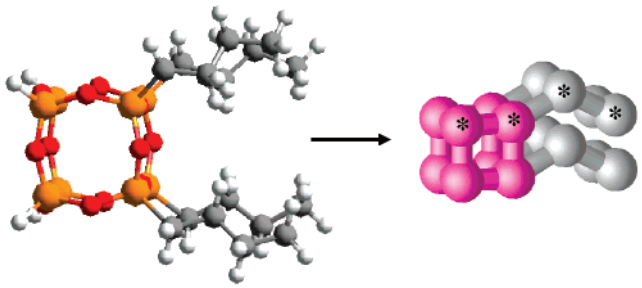

Figure 1. Schematic of the representation of a tetratethered POSS molecule $R'_4R_4Si_8O_{12}$ (left) by our minimal model (right). For example, here R denotes a hydrogen atom and R′ a butyl chain, with one coarse-grained tether monomer approximately representing an ethyl group. The asterisks on the particles in the minimal model may be thought of as denoting monomers constituting a short diblock copolymer chain. The NBB can be regarded as analogous to four diblock copolymers connected by the rigid bonds of the cube or to a surfactant with head and tail groups. In the atomistic representation, the silicon atoms are shown in orange, carbon atoms in gray, oxygen atoms in red, and hydrogen atoms in white.

As a first step toward developing a minimal model of tetratethered POSS molecules, we perform ab initio density functional theory (DFT) calculations to gain insight into the nature of the intermolecular interactions between and structural deformations of the silsesquioxane cages. Such insight will provide us with preliminary guidelines for how to describe the interactions and the cage structure in our minimal model. Here we seek to obtain information on the intermolecular interactions between the nontethered faces of the cages and the extent to which these interactions affect cage structure. The nontethered face is defined by the four nontethered Si corners on each POSS molecule. These corners are typically functionalized with simple nonreactive R groups, such as cyclohexyl rings.[2] Therefore, as one example we study a POSS molecule in which the R groups on the four nontethered corners are cyclohexyl substituents $H_4(C_6H_5)_4Si_8O_{12}$ (cyhex$_4$-POSS). For simplicity, we represent the four tethers (R′ groups) as hydrogen atoms because we are interested primarily in understanding the interactions between the nontethered faces of the cages and the resulting cage distortions. Ab initio calculations on single monotethered POSS molecules with linear alkyl tethers indicate that the tethers do not significantly influence the structure of the silsesquioxane cage,[37] and principal component analysis on the crystal structures of $(CH_3)_8Si_8O_{12}$ and $(C_2H_5)_8Si_8O_{12}$ shows cage deformations of only 3 and 1%, respectively,[38] due to interactions with neighboring cubes. Hence, only intermolecular interactions between the nontethered (cyclohexyl-substituted) sides of the cages are considered in our DFT calculations.

DFT calculations are carried out on systems containing two cyhex$_4$-POSS that are placed at selected dis-

tances in different configurations. The potential energy profiles provide an estimate of the energetic interactions between the nontethered sides of the molecules. In addition to the interaction energies, the electron density distributions around the cyhex$_4$-POSS systems are calculated in order to establish the shape of the electron distribution about the POSS cage and help construct an appropriate minimal model that appropriately captures these electronic and geometric features. Periodic plane wave DFT calculations are carried out using the Vienna *Ab Initio* Simulation Package (VASP).[39] Vanderbilt ultrasoft pseudopotentials[40] are employed to simplify the interaction potential between the ion and core electrons, thereby reducing the computational load. A cutoff energy of 396 eV is used to truncate the number of plane waves. The corrections to the exchange-correlation energy are calculated within the generalized gradient approximation using the revised Perdew−Burke−Ernzerhof (RPBE)[41] functional. The electron density and the corresponding electronic energy converge within an energy tolerance of 10^{-4} eV. A cubic unit cell of dimensions 25 Å × 25 Å × 25 Å is chosen to minimize the interactions between molecules in adjacent cells.

The structure of the cyhex$_4$-POSS system is optimized with four cyclohexyl groups placed on the same face of the POSS cage in two different configurations. In the first configuration, the two molecules are aligned so that the four cyclohexyl groups on each face point directly at one another, thereby creating an initial mirror plane between the two POSS structures (Figure S-1a, Supporting Information). This model is referred to as the "in-line" configuration since the cyclohexyl groups and the cages orient themselves along a central axis. The second configuration explored is a "shifted" configuration, where one of the POSS cages is shifted 4 Å (roughly the length of the POSS cage along an edge) in the *z*-direction away from the in-line configuration (Figure S-1b). This shift allows one cyclohexyl group to interact with the neighboring POSS cage at a shorter distance. Studies on the crystal structures of POSS molecules functionalized with one hexyl tether[42] and with solely hydrogen atoms[43] suggest that the molecules prefer to pack in a similar shifted configuration.

The total energies for both the *in-line* and the *shifted* configurations are determined by carrying out structural optimizations for both the cages and their substituents at a series of points where the Si−Si distances between the two cages are held fixed, thus allowing for optimization at fixed distances between the two molecules (denoted as fixed-optimized). A typical optimization of two interacting POSS molecules required about 40 h of CPU time using four nodes on a cluster running two Intel P4 2.4 GHz processors and 2 GB RAM per node.

The electron density distributions are calculated using the DMol^3 package.[44] The basis sets are double numerical with polarization. All electrons are treated explicitly with relativistic corrections to the core electrons.

B. Results and Discussion. 1. Cage Structure. The bond lengths and bond angles for the isolated and the interacting cyhex$_4$-POSS molecules are listed in Table 1. The structural changes that occur in both the *in-line* and *shifted* configurations as a result of the interactions between the two POSS molecules are determined by comparing the isolated and optimized structures at the interaction distances of 14.5 and 13.5 Å, respectively. These distances are the points where

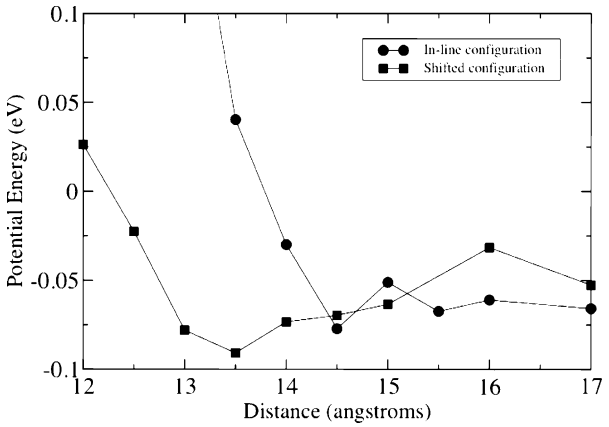

Figure 2. Potential energy curves obtained from DFT calculations for the in-line and the shifted configurations using VASP.

Table 1. Optimized Bond Lengths and Bond Angles for Isolated and Interacting Cyhex$_4$-POSS Molecules

	isolated	in-line 14.5 Å	shifted 13.5 Å
Si−O (Å)	1.625−1.645	1.622−1.649	1.622−1.649
Si−O−Si (deg)	141.8−154.2	141.3−154.8	141.4−155.1
O−Si−O (deg)	108.3−111.0	108.3−110.9	108.2−110.8

the potential energy minima reside (Figure 2). The Si−O bond lengths differ by less than 1 pm, and the Si−O−Si and O−Si−O bond angles by no more than 1°, between the isolated and the interacting molecules in the in-line configuration. Similar to the in-line case, the Si−O bond lengths differ by less than 1 pm, and the Si−O−Si and O−Si−O bond angles vary by no more than 1°, between the isolated molecule and the interacting molecules in the shifted configuration. The negligible differences in the cage bond lengths and bond angles between the isolated and interacting molecules suggest that there is very little distortion of the cages due to cage−cage interaction.

The electron density distributions about the hydrido-POSS and cyhex$_4$-POSS systems are shown in Figure 3 in order to establish the overall shape of the electron density about the cube. In both cases, the electron density extends around the cube structure. There is some degree of "blurring" of the underlying structure that occurs due to electron screening, but both the hydrido-POSS cage and the cyhex$_4$-POSS structures can still be regarded as maintaining a cubic form. As such, for developing a more coarse-grained model, it is reasonable to make an approximation that the POSS molecule remains rigid and cubic.

2. Intermolecular Interactions. The DFT-calculated potential energy curves for the *in-line* and *shifted* configurations are shown in Figure 2. There is a minimum in each potential energy curve that represents the most energetically stable configuration. The energy difference between the minimum and the plateau region is the potential well depth representing the interaction energy strength between the two molecules. The DFT results show that the potential well depth for the in-line configuration is 0.075 eV. The energy minimum occurs at a separation distance of 14.5 Å. The shifted configuration exhibits a potential energy minimum at a separation distance of 13.5 Å and has a potential well depth of 0.09 eV. The small well depths for these systems are indicative of very weak, attractive intermolecular interactions. DFT methods, however, are known to underpredict these weak van der Waals (vdW)

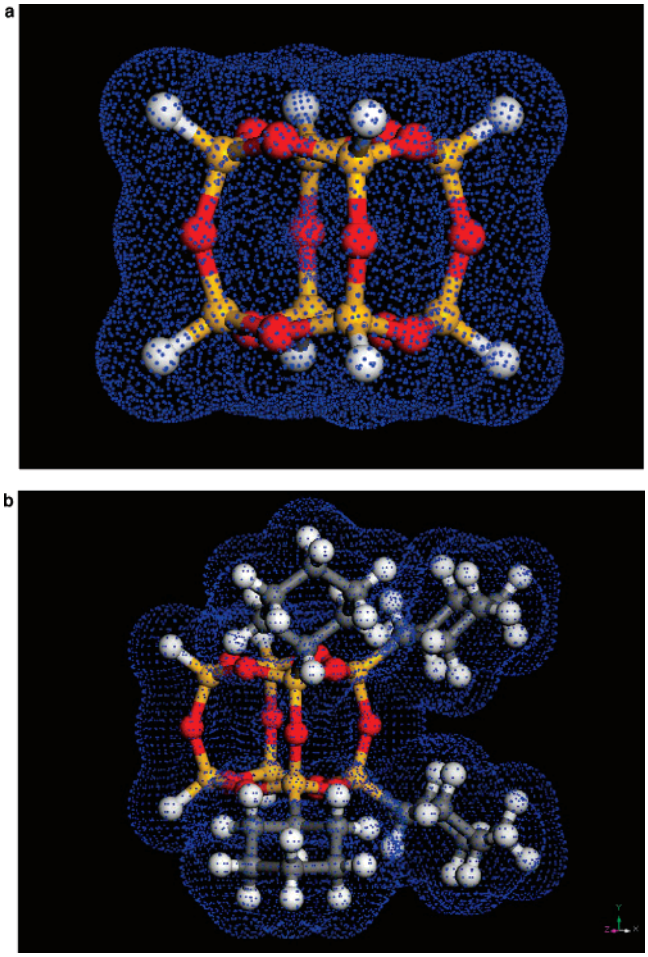

Figure 3. Electron density distribution of (a) hydrido-POSS and (b) cyhex$_4$-POSS.

interactions,[45] so it is possible that the actual interaction energies may be slightly higher. However, previous theoretical calculations for the interactions between two hydrido-POSS cubes are consistent with those produced from simulations that employed a force field derived from an experimental force field for silica.[46]

To summarize, the three key features established from the ab initio calculations that will be used in the development of a preliminary minimal model are that (1) there is very little distortion in the structures of interacting functionalized POSS molecules, (2) the electron density distribution of POSS remains cubic in form for both the "bare" hydrido-functionalized cage and the organic tethered systems, and thus the cubes may be treated as rigid, and (3) there is a weak attraction between POSS cubes with a preferred minimum intercube distance.

C. Model Construction. 1. Cage Structure. We have developed a preliminary coarse-grained model of a tetratethered POSS molecule $R'_4R_4Si_8O_{12}$ as a tethered cubic NBB. The results of our ab initio calculations on interacting cyhex$_4$-POSS molecules are utilized here to guide the construction of a simple, minimal model that captures some of the general features of interacting tetratethered POSS molecules. Currently, our model is not intended to be a specific mapping of a particular NBB. However, such a mapping could be accomplished from further information obtained from quantum mechanical calculations and atomistic simulations employing a highly accurate force field for simulating the intermolecular interactions in these systems, in both the presence and absence of solvent, and will be the subject of future studies.

Because our ab initio calculations show that there is very little distortion in the bond lengths and bond angles of the silsesquioxane cages when the interaction between two tetrasubstituted POSS molecules occurs on the nontethered faces and that the electron density distributions about the cages are cubic in form, we model the cage as a rigid cube with eight beads comprising the cube vertices and connected by perfectly rigid bonds (Figure 1). Each bead represents groups of atoms on the silsesquioxane cage. For simplicity, we assume in our model that the nontether R substituents can be grouped together with atoms that are represented by the vertices of the cube in our minimal model. A rigid cube approximation of the cage structure has been employed in simulations of octafunctionalized POSS−polymer networks[29] and successfully reproduced physical properties of the systems in agreement with experiments.

2. Tethers. Each homopolymer tether on the NBB is modeled as a chain of soft spheres or monomers attached by an attractive potential. In this bead−spring model, each monomer represents a part of the polymer proportional to the persistence length. Pairs of successive monomers along a chain interact via a finitely extensible nonlinear elastic (FENE)[47] anharmonic spring potential

$$U_{\mathrm{FENE}}(r) = \begin{cases} -0.5kR_0 \ln\left[1 - \left(\dfrac{r}{R_0}\right)^2\right] & r < R_0 \\ \infty & r \geq R_0 \end{cases} \quad (1)$$

where r is the distance between neighboring monomers and k and R_0 are the energy and length parameters of the potential. These parameters are assigned the values $k = 30$ and $R_0 = 1.5\sigma$ to ensure relatively stiff bonds while avoiding very high-frequency modes and chain crossing.

Our proposed tethered POSS building block can be regarded as an analogue to linear diblock copolymer and surfactant molecules. The NBB can be thought of as either four short diblock copolymers that are attached together by the rigid bonds of the cage (Figure 1) or a surfactant molecule with an effective "head" group represented by the cube and a "tail" group comprised of the four tethers.

3. Modeling Immiscibility for Self-Assembly Studies. To simulate phase separation arising from selectivity of the implicit solvent for cube beads or tether monomers, we denote the interactions as the following.[30,48−51] If the solvent is *poor* for one particle species, then that species will interact via an attractive potential. Conversely, if the solvent is *good* for a particular species, then that species will interact via a purely repulsive potential. As the cube beads and tether monomers are considered different species, they also interact via this purely excluded-volume interaction to mimic immiscibility between them.

We choose to model interactions between cubes as attractive based on the weak, attractive interactions observed in our DFT calculations of two interacting cyhex$_4$-POSS molecules. Experimental studies of POSS−polymer copolymer systems[19,20] also suggest the presence of attractive interactions between the silsesquioxane cubes, as these systems exhibit a tendency to phase

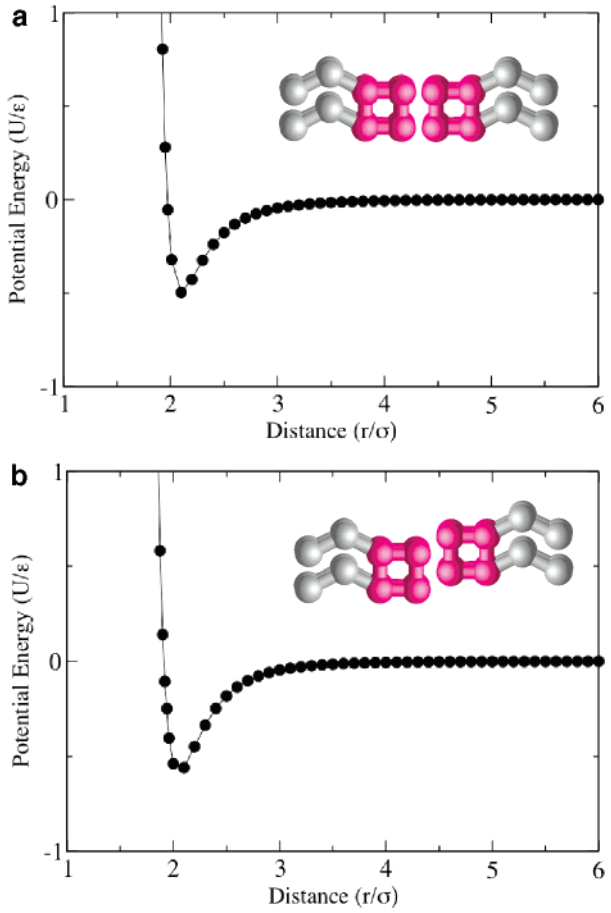

Figure 4. Site−site potential energy curves for two interacting minimal model nanocubes aligned in (a) the in-line and (b) the shifted configurations. The energies shown are based on the Lennard-Jones 12−6 potential with $\epsilon = 1$ and are plotted as a function of the distance between cube centers.

segregate. We approximate these interactions using the simple Lennard-Jones (LJ) 12−6 potential,[52] which accounts for both excluded-volume and vdW interactions. In our simulations, we use a truncated and shifted site−site LJ potential between corner beads of two cubes:

$$U_{\mathrm{LJ}}(r) = 4\epsilon\left[\left(\frac{\sigma}{r}\right)^{12} - \left(\frac{\sigma}{r}\right)^{6} - \left(\frac{\sigma}{r_c}\right)^{12} + \left(\frac{\sigma}{r_c}\right)^{6}\right] - (r - r_c)\left(\frac{\mathrm{d}U_{\mathrm{LJ}}(r)}{\mathrm{d}r}\right)_{r=r_c} \qquad r \le r_c \quad (2)$$

where $r_c = 2.5\sigma$ is the cutoff distance beyond which the interaction is set to zero and r is the distance between two beads.

Figure 4 shows the site−site intermolecular potential energies between two minimal cubes as a function of the distance between cube centers. The two cubes were aligned in the in-line and shifted configurations, which are analogous to those studied in the DFT calculations. The potential energy curve for the in-line configuration is qualitatively similar to that obtained for the interacting cyhex$_4$-POSS molecules using DFT. The energy curve for the shifted configuration exhibits a slightly deeper well depth, with the minima shifted to a shorter distance, compared to the in-line configuration. The steepness of the repulsion at shorter separation distances for the shifted configuration is slightly less than for the in-line configuration. These trends are in agreement with the DFT calculations. Thus, the site−site LJ potential appears suitable here for capturing the attractive interactions between cubes. It is also used to portray the site−site interactions between two tether monomers to model the situation when the implicit solvent is poor for that species.

The site−site interactions between cube beads and tether monomers are modeled by a purely repulsive Weeks−Chandler−Andersen[53] (WCA) soft-sphere potential

$$U_{\mathrm{WCA}}(r) = 4\epsilon\left[\left(\frac{\sigma}{r}\right)^{12} - \left(\frac{\sigma}{r}\right)^{6}\right] + \epsilon \qquad r \le r_c \quad (3)$$

where $r_c = 2^{1/6}\sigma$. This potential is intended to mimic immiscibility between the different species.

The depth of the attractive well ϵ, in connection with the temperature T, controls the role of the interaction parameter χ in the Flory−Huggins lattice mean-field model. χ is related to the solvent quality and the degree of immiscibility among bead types, and it is inversely proportional to temperature $\chi \sim \epsilon/k_B T$, where k_B is Boltzmann's constant.

In summary, we have constructed a preliminary minimal model of a tetratethered POSS molecule in which the silsesquioxane cage is represented as a rigid cube, polymeric tethers are approximated as bead−spring chains, and weak attractive intermolecular interactions between cages are described by the LJ potential. We emphasize that the results of our ab initio calculations on interacting cyhex$_4$-POSS molecules provide us with guidelines for developing a simple model that captures some of the general features of interacting tetratethered POSS molecules.

III. Tetratethered Nanocube Self-Assembly

A. Methodology. To study tetratethered nanocube self-assembly, we employ a stochastic molecular dynamics simulation method[54,55] that treats certain solvent effects implicitly, thereby enabling investigations of assembly in solution. The equation of motion for each monomer i is

$$m_i \dot{\mathbf{v}}_i(t) = -m_i \xi_i \mathbf{v}_i(t) + \mathbf{F}_i(x_i(t)) + \mathbf{R}_i(t) \quad (4)$$

where m_i is the mass of monomer i, and $\mathbf{x}_i$, $\mathbf{v}_i$, $\mathbf{F}_i$, and ξ_i represent the position, velocity, force, and friction coefficient acting on monomer i, respectively. Equation 4 represents the simplest form of stochastic dynamics in which the time and spatial correlations in the friction coefficient are neglected and is commonly referred to as Brownian dynamics. The random force $\mathbf{R}_i$ is assumed to be stationary, Markovian, and Gaussian with zero mean. It has no correlation with prior velocities or with the conservative force. The amplitude and space-time correlations of $\mathbf{R}_i$ are governed by the fluctuation−dissipation theorem.[56] Thus, $\mathbf{R}_i$ must satisfy the conditions

$$\langle \mathbf{R}_i(t) \rangle = 0$$
$$\langle \mathbf{R}_i(t)\, \mathbf{R}_j(t') \rangle = 6m\xi k_B T \delta_{ij} \delta(t - t') \quad (5)$$

The friction coefficient and stochastic noise term couple the system to a heat bath. The latter term acts as a heat source to compensate for the energy sink due to viscous drag and both quantities together help to stabilize the

numerical errors that accumulate during the course of a long simulation. The stationary solution is the Boltzmann distribution, and hence these simulations sample a canonical (NVT) ensemble.

We use reduced units in which the basic units for length and energy are σ and ϵ of the LJ potential, respectively. Each cube bead and tether monomer has the same size $\sigma = 1$ and mass $m = 1$. We present our results in terms of these reduced units; hence, the reduced temperature is defined as $T^* = k_BT/\epsilon$, the interaction energy parameter as $\epsilon^* = \epsilon/k_BT$, the reduced time step as $\Delta t = t/\sigma\sqrt{m/\epsilon}$, and the reduced friction coefficient as $\xi^* = \xi\sigma\sqrt{m/\epsilon}$. The concentration of molecules in the system is based on the reduced number density of particles $\rho^* = N\sigma^3/V$, where N denotes the total number (sum) of cube beads and tether monomers and V is the volume of the simulation box. The volume or packing fraction ϕ of molecules in the system is determined from the number density.

We simulate systems of $Nb = 400$ and 1000 NBBs having polymer tethers each consisting of $Nt = 2$ monomers ($N = 6400$ and 16 000, respectively) and $Nt = 4$ monomers ($N = 9600$ and 24 000, respectively) using cubic simulation cells and periodic boundary conditions. The equations of motion are integrated using the leap-frog algorithm[52] with time step $\Delta t = 0.01$. ξ^* is set to unity for each monomer so that our simulations are performed in the range between overdamped and purely deterministic regimes.[50] We employ the method of quaternions[52] to simulate rigid-body motion of the cube. The concentration of NBBs is varied to simulate systems in solvent and in the melt. Each system is initially relaxed athermally (i.e., only excluded-volume interactions, $\epsilon^* = 0$) into a disordered configuration and subsequently cooled in small increments $\Delta\epsilon^* \leq 0.1$. Once the systems have evolved into highly ordered structures, we reverse the path by heating the systems again in small increments $-\Delta\epsilon^* \leq 0.1$. In these procedures, the last equilibrated configuration at ϵ^* is used as the first configuration at $\epsilon^* \pm \Delta\epsilon^*$, and runs are performed until the system has reached equilibration at each ϵ^*. The annealing process is used to locate the order−disorder transitions (ODTs) in our systems by examining interaction energies between monomer types and tether mean-squared corner-to-end (cube corner bead to last backbone monomer on the tether) distance as a function of ϵ^*.[57,58] The ODTs are taken to be the values of ϵ^* immediately preceding the discontinuous or sharp changes in interaction energies upon cooling of the system. Because the final assembled structures could depend on the annealing history, we also instantaneously cool or quench the initial athermal configurations to low temperatures to verify that the same structures form. We monitor the structural evolution of the systems as a function of time by inspecting snapshots of configurations, which we use later to calculate various structural quantities described below.

For the systems containing micelles at low concentration, equilibrium micellar sizes and shapes are monitored during the simulation to investigate their structural characteristics. The size M of an aggregate is defined as the number of NBBs it contains. A NBB is designated as belonging to an aggregate if the position of its cube center is within the distance of the cube center position of a neighboring molecule according to the LJ interaction distance between cube corner beads on each molecule[52,59] ($r_{cluster} = 2.5\sigma$). The volume fraction ϕ_M of a micelle of size M is based on the total number of cube corner beads and tether monomers N_{site} in the micelle. The shapes of the micelles are characterized by calculating the three principal radii of gyration and the asphericity parameter.[60−62] The three principal radii of gyration R_1, R_2, and R_3 (in descending order) are the eigenvalues of the radius of gyration tensor defined by

$$R_{\gamma\sigma} = \left[\frac{1}{N_{site}}\sum_{i=1}^{N_{site}}(\gamma_i - \gamma_{com})(\delta_i - \delta_{com})\right]^{1/2} \quad (6)$$

where γ and δ are the x, y, z coordinates of particles in the micelle and γ_{com} and δ_{com} are the x, y, z coordinates of the center of mass of the micelle. The asphericity parameter is defined as

$$A_s = \frac{\sum_{i>j}^{d}\langle(R_i^2 - R_j^2)^2\rangle}{(d-1)\langle(\sum_{i=1}^{d}R_i^2)^2\rangle} \quad (7)$$

for a d-dimensional aggregate and $1 \leq i \leq d$.

We investigate two types of solvent conditions: (1) the solvent is good for the tether monomers and poor for the cube beads, i.e., cube−cube (CC) interactions are of the LJ type, and tether−tether (TT) and cube−tether (CT) interactions are both of the WCA type, and (2) the solvent is neutral and poor for both species, i.e., CC and TT interactions are both of the LJ type while CT interactions are of the WCA type.

B. Results and Discussion. B1. Self-Assembly of Tethered NBBs with $Nt = 2$. 1. High Concentrations ($\rho^* > 0.5$, $\phi > 0.25$). Figure 5 shows snapshots of equilibrium configurations from a system of $Nb = 1000$ tethered cubic NBBs with $Nt = 2$ at $\rho^* = 0.86$ ($\phi = 0.45$) and $\epsilon^* = 0.8$ in selective solvent that is good for the tethers and poor for the cubes. This concentration corresponds to the melt state. The selective solvent condition is chosen because solvent selectivity strongly influences phase transitions in solutions of block copolymers. We observe assembly of the building blocks into hexagonally arranged cylindrical or columnar phases of cubic cross section, with the cubes comprising the core and the tethers pointing outward. The simulation required roughly 250 CPU hours on a single Athlon AMD 2400 processor for the structures to form. The cubic packing of the NBBs within each cylinder can be attributed to the cubic geometry of the NBB core and demonstrates the ability to manipulate the shape of the final assembled structures from round to cubic by merely attaching NBBs with a specific geometry to polymer chains. The cubic NBB cores appear to pack primarily in a shifted face-to-face arrangement within the cylinders. Thus, our model captures features of local packing observed in POSS systems.[42,43]

We also find that the cylinders are tilted in both the small and large systems. The tilt is induced by the finite size of the cubic simulation boxes and raises the question of the extent to which the box sizes affect the assembly of the NBBs into the correct equilibrium structures. The periodicity of the structures may not be exactly commensurate with the size of the simulation box, and it is possible that the resulting structures could deviate from the preferred morphologies to satisfy the periodic conditions. However, we observe here that the

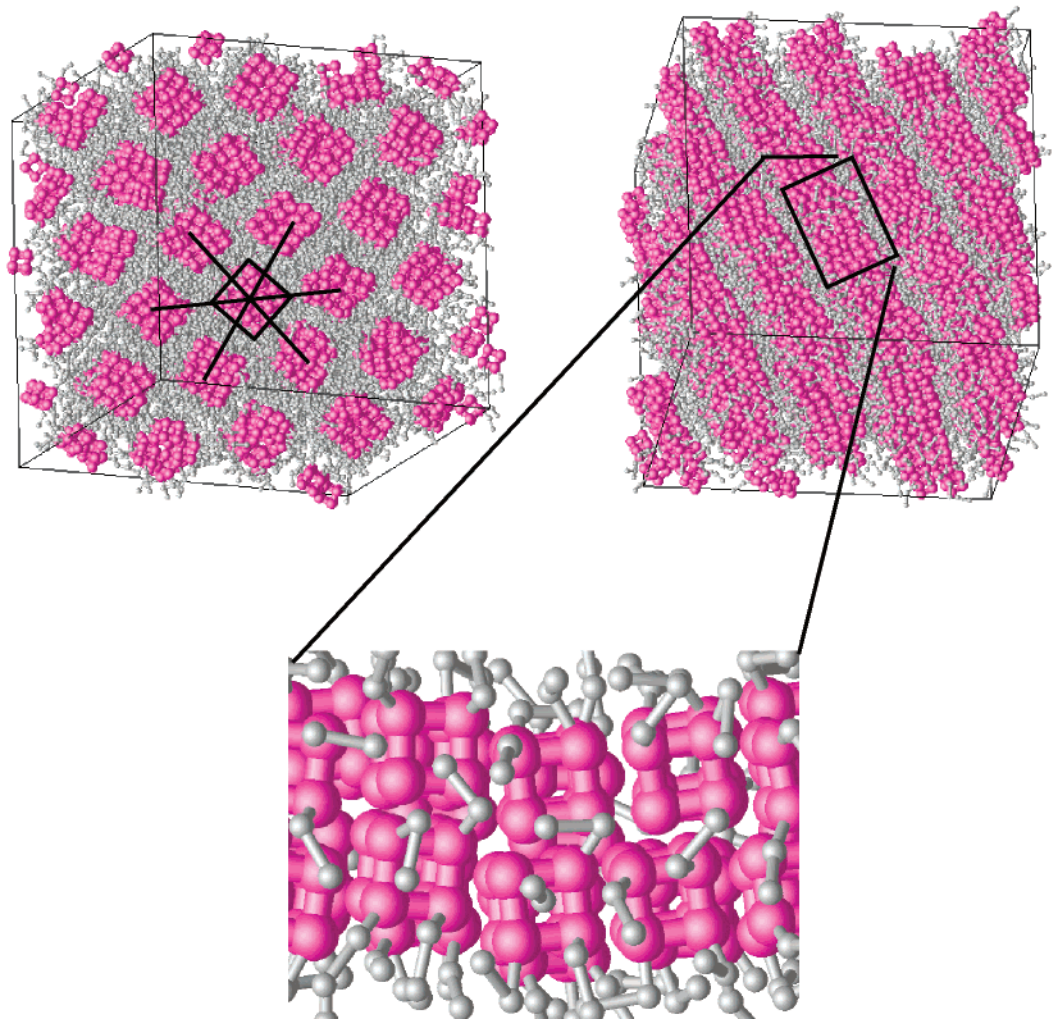

Figure 5. End and side views of final equilibrium configuration obtained via cooling for the $Nb = 1000$, $Nt = 2$, $\rho^* = 0.86$ ($\phi = 0.45$), $\epsilon^* = 0.8$ system. The lines drawn in are provided as guides to the eye for visualizing the hexagonal arrangement of cylinders and the cubic geometry of the assembled structures. The tether monomers are reduced in size here for clarity. A magnified view of one self-assembled cylinder illustrates the local packing of the NBBs.

Table 2. Properties of $Nt = 2$ Tethered NBBs for Different Box Sizes $\rho^* = 0.86$ ($\phi = 0.45$), $\epsilon^* = 0.8$

no. of molecules Nb	morphology	simulation box dimensions (σ)	intercylinder spacings (σ)	potential energy $U_{CC/TT}$ (ϵ)	potential energy U_{CT} (ϵ)
400	cylindrical	19.5 × 19.5 × 19.5	5.87|6.37|6.61	−11.47	1.27
1000	cylindrical	26.5 × 26.5 × 26.5	5.82|6.44|6.40	−11.49	1.27

molecules always self-assemble into the same cylindrical morphology and with nearly the same intercylinder spacings, regardless of the size of the simulation cell (Table 2). Thus, we are confident that the self-assembly of the NBBs into equilibrium cylindrical structures at this state point is correct.

We investigate the ODT of tethered NBBs by monitoring the discontinuous or sharp changes in the interaction energies as a function of ϵ^*. Figure 6a,b show the nonbonded pair interaction energies between the same species (CC and TT) and different species (CT) of beads, $U_{CC/TT}$ and U_{CT}, respectively, during the cooling and heating processes for the system of $Nb = 400$ molecules. The plots illustrate two important features. First, both potential energies exhibit discontinuous changes at $\epsilon^*_{ODT} = 0.75$ upon cooling. On the basis of snapshots of configurations, the drops in $U_{CC/TT}$ and U_{CT} at $\epsilon^*_{ODT} = 0.75$ represent ordering of the molecules into cube-rich and tether-rich phases to form cylindrical structures. Second, upon reheating of the system, a hysteresis in the transition temperature is observed that is characteristic of first-order phase transitions. Thus, the transition from a disordered state to hexagonally packed cylinders of tethered cubes appears first-order at this particular temperature and concentration, as in traditional block copolymer and surfactant systems; however, additional calculations outside the scope of this work are necessary to fully identify the type of transition. To investigate the effect of finite box size on the computed energies, we also calculate $U_{CC/TT}$ and U_{CT} for the larger system of $Nb = 1000$ molecules. Table 2 shows that the corresponding potential energies for each system are in excellent agreement; therefore, the box sizes do not appear to influence the values of the pair interaction energies as expected.

To verify the ODT predicted by the discontinuous changes in the pair interaction energies, we also compute the average tether mean-squared corner-to-end distance R^2 as a function of ϵ^* (Figure 6c). There is again a discontinuous change at $\epsilon^*_{ODT} = 0.75$ upon cooling and hysteresis in R^2 upon reheating of the system. These trends are identical to those observed for the potential

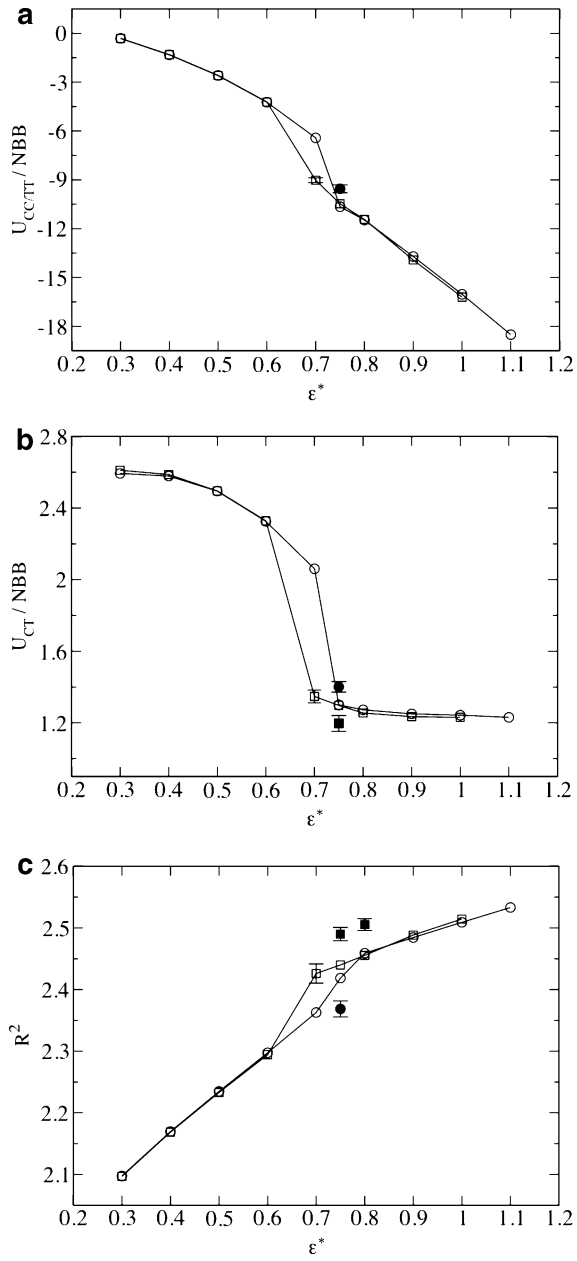

Figure 6. The variation of the nonbonded pair interaction energies per NBB (a) $U_{CT/TT}$/NBB and (b) U_{CT} /NBB with the interaction energy parameter ϵ^* for the system $\rho^* = 0.86$ ($\phi = 0.45$), $Nb = 400$, $Nt = 2$. (c) The variation of the average tether mean-squared corner-to-end distance R^2 with ϵ^*. Open circles and squares denote the corresponding values during cooling and heating, respectively. Error bars are shown when larger than the symbol. Some of the error bars are illustrated by the filled circles and squares above or below the corresponding open symbols for clarity.

energies $U_{CC/TT}$ and U_{CT}. The R^2 data indicate that the polymer tethers gradually stretch with increasing ϵ^*, or lower temperature, to minimize the unfavorable interactions with cube beads and with other tether monomers on different chains to satisfy the selective solvent conditions. The discontinuity in R^2 upon cooling signifies more pronounced stretching of the tethers to facilitate ordering of the molecules into cube-rich and tether-rich phases. Table 3 summarizes the ODT phase boundary at which cylindrical phases form for the concentrations studied here.

2. Low Concentrations ($\rho^* < 0.5$, $\phi < 0.3$). For systems at low concentration in solvent that is selectively good for the tethers and poor for the cubes, we find that the tethered NBBs self-assemble into spherical and elongated micellar phases instead of cylindrical phases. We study sufficiently large systems of $Nb = 1000$ NBBs ($N = 16\,000$) to ensure that any three-dimensional periodicity present in the equilibrium morphology is captured. Figure 7 shows the aggregate size distributions for $\rho^* = 0.48$ ($\phi = 0.25$) at various values of ϵ^*. At $\epsilon^* = 0.1$, corresponding to high temperature, the distribution is a sharply decreasing function of aggregate size M. Individual NBBs that do not belong to a micelle, denoted here as *unimers*, coexist with small and short-lived aggregates (e.g., dimers and trimers). As ϵ^* increases, or temperature decreases, short-lived aggregates of larger size begin to form. The aggregate size distribution is still monotonically decreasing with M but becomes broader. At $\epsilon^* = 0.5$, larger aggregates continue to form, and at $\epsilon^* = 0.7$, a second peak appears in the distribution that corresponds to the formation of micelles. This micellar peak grows higher and moves to larger values of M with further increases in ϵ^*. The trends in the aggregate size distribution at various ϵ^* for our tethered cubic NBB system have also been observed in simulation studies of self-assembling amphiphiles in solution.[63] The aggregate size distribution is asymmetrical around the micellar peak and is caused by the growth of micelles at higher M.[62]

Table 3. Order−Disorder Transitions for Cylindrical Morphologies in $Nb = 400$ Systems

Nt	concn ρ^*	ϵ^*_{ODT}	Nt	concn ρ^*	ϵ^*_{ODT}
2	0.57	1.33	2	0.86	0.75
2	0.67	1.05	4	0.76	0.9
2	0.76	0.85	4	0.86	0.77

The principal radii of gyration and asphericity parameter results for the system at $\rho^* = 0.48$ and $\epsilon^* = 1.2$ are presented in Figure 8. The three principal radii increase with aggregate size and are similar in value, although not equal, for aggregates having less than 11 NBBs. Furthermore, these aggregates (with the exception of $M = 2$ and $M = 3$) have asphericity parameter values less than the maximum value of 0.1 that characterizes spherical objects.[63] Thus, micelles containing up to approximately $M = 11$ NBBs have a roughly spherical geometry. Snapshots of configurations reveal that the micelles consist of the cubes assembled in the core and the tethers pointing outward in accordance with the selective solvent condition. For aggregate sizes between $M = 12$ and $M = 29$, the smallest two principal radii R_2 and R_3 are approximately equal while the

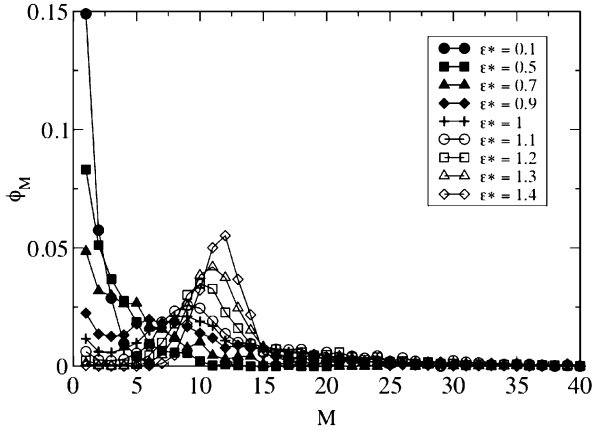

Figure 7. Aggregate size distributions for a system of $Nb = 1000$ NBBs with $Nt = 2$ at concentration $\rho^* = 0.48$ ($\phi = 0.25$).

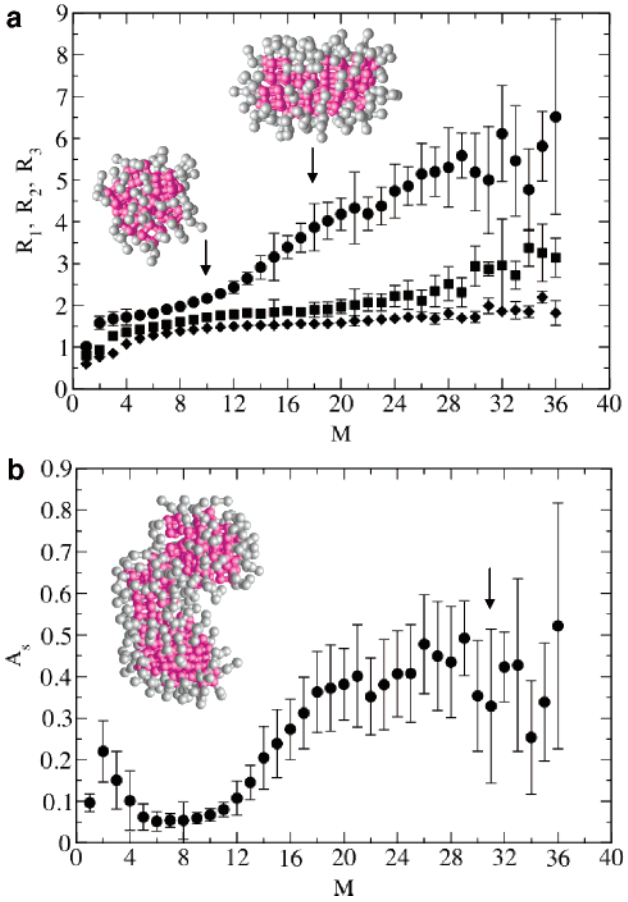

Figure 8. The shapes of micelles in a system of $Nb = 1000$ NBBs with $Nt = 2$ at concentration $\rho^* = 0.48$ ($\phi = 0.25$) and $\epsilon^* = 1.2$. (a) Principal radii of gyration. (b) Asphericity parameter. Error bars are shown when larger than the symbol. Arrows indicate the sizes of the micelles pictured in the inset.

largest one R_1 increases roughly linearly with increasing M. These results indicate that the micelles are growing in one direction to form elongated or cylindrical structures. The asphericity parameter increases from about 0.1 at $M = 12$ to 0.5 at $M = 29$. It appears that the cubic shape of the NBB facilitates the formation of the cylindrical micelles, with the tethered molecules preferring to pack face-to-face within these structures. Coalescence of two micelles into larger wormy micelles is observed. For large micelles of size $M > 29$, the values of the largest principal radius R_1 and the asphericity parameter fluctuate as M increases. The fluctuations are due to poor statistics at these values of M.

We investigate ordering of the micelles by simulating several system sizes having $Nb = 32$, 256, 400, and 1000 tethered NBBs. We find that disordered spherical micelles exist at dilute concentrations for all system sizes. The micelles order into a face-centered-cubic (fcc) pattern at higher concentrations $\rho^* = 0.29$ ($\phi = 0.15$), 0.38 ($\phi = 0.2$), and 0.48 ($\phi = 0.25$) for simulations with $Nb = 32$. Only one unit cell of the fcc lattice exists in this small simulation box. The micelles are all essentially spherical in shape. To test whether the ordering is an artifact of the small box size, this system was replicated in three dimensions to produce a larger system with $Nb = 256$. This latter system was subsequently simulated at the same value of ϵ^* as for the smaller system. Inspection of simulation snapshots indicates that the fcc pattern persists in this bigger system, with the micelles remaining spherical. However, even this system is still quite small, so we also simulated independent systems of $Nb = 400$ and $Nb = 1000$ NBBs. We find that true fcc ordering becomes much less pronounced in these larger systems and is sensitive to the cooling rate or quench depth. Instead of the NBBs assembling into solely spherical micelles, spherical micelles form for low M and elongated or cylindrical micelles form at higher M. The cylindrical or wormy micelles arise from the growth of micelles at higher M due to coalescence of adjacent micelles into larger aggregates. The short tethers do not appear to provide a thick enough corona to shield the micellar cores comprised of cubes. As a result, the cubes in one micelle have a propensity to agglomerate with cubes in other micelles when they are brought close together. Furthermore, the elongated micelles may be favorable because interactions between the short solvophilic tethers and the solvophobic core are avoided in this nonspherical geometry. The tether monomers are essentially excluded from the solvophobic core here. Thus, the free energy is minimized, albeit at the expense of an increase in the surface free energy resulting from pushing of the tether monomers outward away from the core.[64] A similar behavior was observed in simulations of coarse-grained hydrophobic/amphiliphic copolymers.[65]

The assembly of these cylindrical micelles are favored at higher values of ϵ^* or lower temperatures. If we cool a system of disordered tethered NBBs instantaneously to substantially lower temperatures instead of in small increments of ϵ^*, we find that self-assembly tends to result in the formation of elongated micelles that are disordered. Altogether, these findings imply that the fcc ordering of micelles found in the smaller system sizes at these concentrations is probably an artifact of the small box sizes. We surmise that if we were able to simulate systems significantly larger than $Nb = 1000$ NBBs at these concentrations, elongated micelles would always tend to form over time and assume many different orientations that would not result in a higher level of intermicellar ordering.

B2. Self-Assembly of Tethered NBBs with $Nt = 4$. To investigate the effect of tether length on the self-assembly behavior of the cubic NBBs, we perform simulations of $Nb = 400$ and 1000 NBBs ($N = 9600$ and 24 000, respectively) with longer tethers each consisting of $Nt = 4$ monomers under selective solvent conditions. We find that the tethered NBBs self-assemble into hexagonally arranged cylindrical or columnar morphologies at very high concentrations $\rho^* = 0.76$ ($\phi = 0.4$) and $\rho^* = 0.86$ ($\phi = 0.45$) that correspond to the melt state. At lower concentrations $\rho^* < 0.7$ ($\phi < 0.4$), the NBBs prefer to self-assemble into micelles. We compute the nonbonded pair interaction energies $U_{CC/TT}$ and U_{CT}, and tether mean-squared corner-to-end distance R^2, as a function of ϵ^* to locate the ODT phase boundary at various concentrations. These results are summarized in Table 3.

In the range of concentrations $\rho^* = 0.29$ to $\rho^* = 0.67$ ($\phi = 0.15$ to $\phi = 0.35$, respectively), the tethered NBBs self-assemble into micelles that are ordered in an fcc-like packing. The aggregate size distribution at $\rho^* = 0.48$ for various values of ϵ^* is presented in Figure 9. At high values of ϵ^*, unimers and small aggregates are prevalent in the system. We observe the emergence of a second micellar peak at $\epsilon^* = 0.7$ with further increases in ϵ^* or at lower temperatures. This peak grows higher and moves to larger aggregate sizes M at even larger

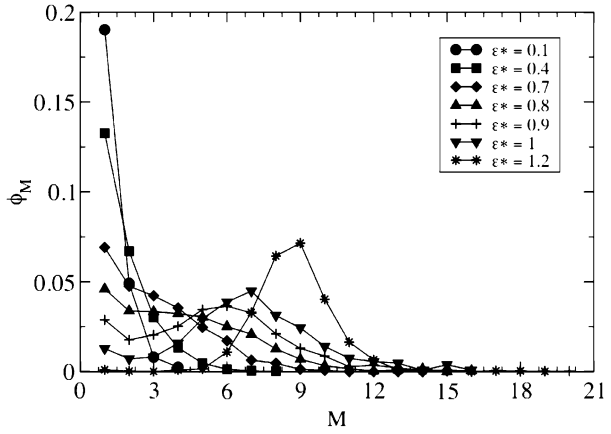

Figure 9. Aggregate size distributions for a system of $Nb = 400$ NBBs with $Nt = 4$ at concentration $\rho^* = 0.48$ ($\phi = 0.25$).

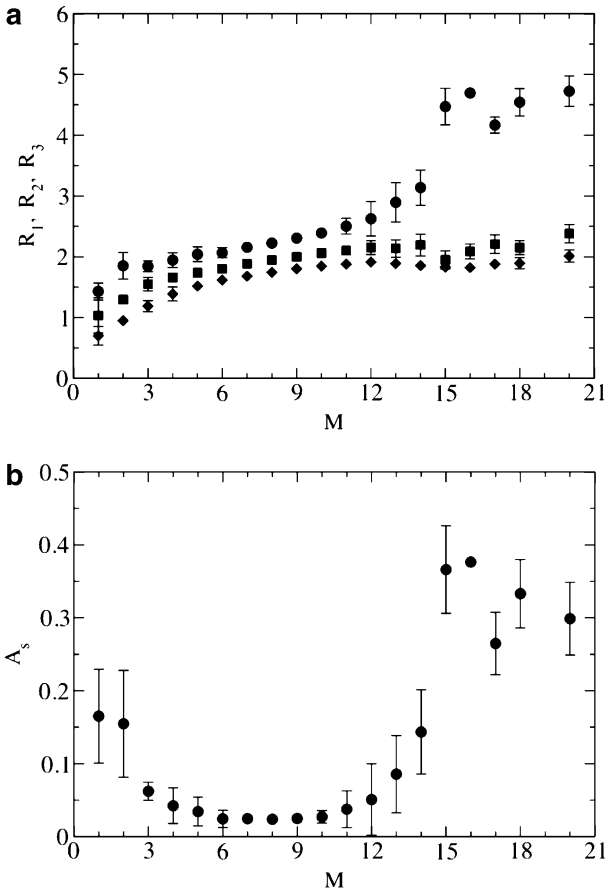

Figure 10. The shapes of micelles in a system of $Nb = 400$ NBBs with $Nt = 4$ at concentration $\rho^* = 0.48$ ($\phi = 0.25$) and $\epsilon^* = 1.2$. (a) Principal radii of gyration. (b) Asphericity parameter. Error bars are shown when larger than the symbol.

values of ϵ^*. The principal radii of gyration and asphericity parameter are shown in Figure 10 as a function of M. The three principal radii increase with M and track each other over the range of aggregate sizes for which the statistics are good. The value of the asphericity parameter is less than 0.1 for these values of M. Thus, the longer solvophilic tethers on the NBB induce more curvature in the self-assembled structures, leading to micelles that are essentially spherical in shape.

The longer tether lengths also increase the thickness of the micellar corona, which contains primarily tether monomers. The stronger excluded-volume effects between adjacent micelles resulting from the larger coronas consisting of swollen, flexible tethers and crowding of the micelles at the higher concentrations appear to facilitate ordering of the structures. We observe in snapshots of simulated configurations that the fcc arrangement of the micelles becomes more refined, and thus more easily distinguishable, as the tether length increases. The packing persists in different size systems and appears stable here, unlike the systems of NBBs with $Nt = 2$ that exhibited loss of ordering with increasing system size.

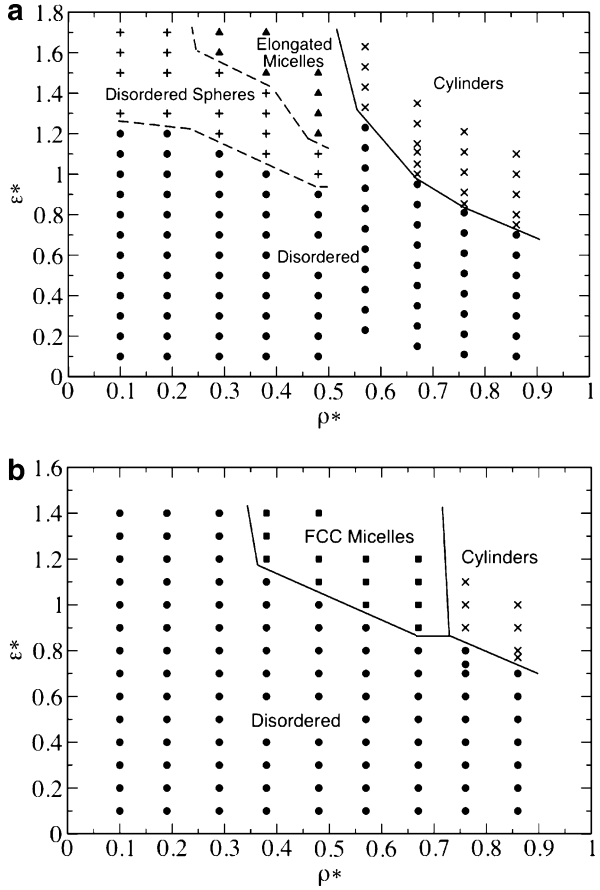

Figure 11. Proposed phase diagrams for systems of tethered cubic NBBs studied here. Symbols correspond to simulated state points and the different morphologies observed. Phase boundaries are drawn as guides to the eye. (a) $Nt = 2$; (b) $Nt = 4$.

The assembly of the NBBs into a fcc pattern contrasts with the typical self-assembly of diblock copolymers and surfactants into body-centered-cubic (bcc) ordered patterns at low concentrations. The fcc packing observed here may be related to the short-ranged interaction between tether monomers, leading to ordering of the micelles at the best packing efficiency that accommodates their high packing density. Diblock copolymers in solvent have been shown to favor fcc packing over bcc ordering as the repulsive interactions between micelles becomes increasingly short ranged.[66]

B3. Phase Diagrams. 1. NBBs with $Nt = 2$. On the basis of the values of ϵ^*_{ODT} obtained for systems of tethered NBBs at high concentration and the micellar behavior of the systems at low concentration, we construct a semiquantitative phase diagram for the $Nt = 2$ molecule, as shown in Figure 11a. For high concentrations $0.5 < \rho^* < 0.9$ ($0.3 \leq \phi \leq 0.45$), the ODT points demarcate a boundary between regimes where the systems are in a disordered state and where they are

ordered into hexagonally packed cylindrical phases. At lower concentrations $\rho^* < 0.5$ ($\phi \leq 0.25$), the molecules self-assemble into disordered micelles that are either spherical or elongated in shape. Both spherical (low M) and elongated micelles (higher M) exist in the range of concentrations $0.3 \leq \rho^* \leq 0.5$ ($0.15 \leq \phi \leq 0.25$). At more dilute concentrations, the tethered NBBs self-assemble into disordered spheres. We delineate these two types of micellar regions on the phase diagram.

Because the tethered NBB studied here can be regarded as an analogue to a surfactant or amphiphilic molecule with a head group H and tail group T′, it is instructive to compare the proposed phase diagram for our molecule with the phase behavior of linear surfactants predicted by simulation. In solvent that is selectively good for the tethers and poor for the cubes, i.e., the tethers T are solvophilic and the cubes C are solvophobic, a tethered NBB has a head group corresponding to the cube and a tail group corresponding to the four tethers. For example, if the solvent is water, we take the cube to be more hydrophobic than the tethers based on experiments of POSS molecules in solution.[24,25] A single tetratethered cubic NBB with eight cube corner beads and four tethers each with $Nt = 2$ monomers has composition C_8T_8, or can be thought of as four C_2T_2 chains (see Figure 1), and is thereby enthalpically equivalent to a linear and compositionally symmetric surfactant $H_iT'_j$ ($i = j$). If we compare our proposed phase diagram for the tethered cubic NBB with that of an $H_4T'_4$ surfactant in water (H is solvophilic and T′ is solvophobic for the surfactant) that was previously produced from lattice Monte Carlo simulation,[57] we observe qualitative similarities between the phase diagrams for the two systems. There are regions in which each system self-assembles into disordered spherical and elongated micelles at low concentration ($\rho^* < 0.29$ here; $C_A < 0.45$ in ref 57) and into hexagonally packed cylinders at higher concentration ($0.5 < \rho^*$ here; $0.45 \leq C_A \leq 0.68$ in ref 57). For the tethered NBB, no investigations were made into the potential self-assembly of the molecules into the cubic gyroid and rhombohedral-like mesh intermediate phases observed in surfactant self-assembly because ordering into these patterns is extremely sensitive to the dimensions of the simulation box and occurs only if the box size is very close to the preferred size.

We anticipated ordering of the tethered NBBs at very high concentrations into a lamellar phase, but this is not observed. A lamellar phase typically evolves in systems of compositionally symmetric surfactants and diblock copolymers. The absence of this phase in the system studied here is attributed to the unique architecture of the tethered cubic NBB. Although the molecule is compositionally equivalent to that of a symmetric surfactant or diblock copolymer, the polymer tethers are each attached to the cube at four different junction points. This connectivity differs significantly from how two different polymer species or blocks are connected in linear surfactant or diblock copolymers; namely, the different species are connected to each other at a single junction point occurring at one chain end of each species. The connectivity of the four tethers to the cube, coupled with the flexibility of the tethers and swelling of the tethers due to the favorable interactions between tethers and implicit solvent, results in the chains orienting themselves in different directions relative to the face of the cube to which they are attached. The four tethers are very rarely all oriented perpendicular to the face of the cube to which they are attached, as depicted in Figure 1. Hence, the polymer chains on a single tethered NBB exclude a large amount of free volume that inhibits self-assembly of the cubes into the lamellar phase.

We also perform simulations of tethered NBBs in solvent that is neutral and poor for both the cube and the tether species to investigate whether the formation of a lamellar phase is dependent on the solvent conditions. No lamellar morphologies are observed based on snapshots of simulated configurations. We only observe self-assembly of the molecules into hexagonally arranged cylindrical phases at the same values of concentration that these phases were found under the selective solvent conditions. Ordering of the system into these structures under neutral solvent conditions simply occurs faster (i.e., in a smaller number of simulation time steps) due to the stronger driving force arising from CC and TT interactions now both being of the attractive LJ type.

2. NBBs with $Nt = 4$. We construct a semiquantitative phase diagram for the $Nt = 4$ molecule (Figure 11b) based on the values of ϵ^*_{ODT} obtained for systems of tethered NBBs at high concentration and the micellar behavior of the systems at low concentration. For high concentrations $0.7 < \rho^* < 0.9$ ($0.4 \leq \phi \leq 0.45$), the ODT points demarcate a boundary between regimes where the systems are in a disordered state and where they are ordered into hexagonally packed cylindrical phases. At low concentrations $\rho^* < 0.7$ ($\phi \leq 0.35$), the molecules self-assemble into spherical micelles. The micelles order into a fcc-like pattern over a large range of concentrations $0.29 \leq \rho^* \leq 0.67$ ($0.15 \leq \phi \leq 0.35$). We construct the branch of the phase boundary at low concentrations to distinguish this region on the phase diagram. No lamellar phases were observed in simulations of this molecule.

Comparing the $Nt = 2$ and $Nt = 4$ phase diagrams for the tetratethered cubic NBB, we find that the longer tether length (i.e., longer solvophilic group) decreases the concentration regime in which hexagonally arranged cylindrical structures form and broadens the range of concentrations in which micelles form. The loss or decrease of morphologies at large concentrations, and the appearance of an increasing ordered micellar phase, with increasing length of the solvophilic group was previously observed in simulations of surfactant solutions.[67] The fcc-like ordering of micelles for NBBs with $Nt = 4$ occurs over a substantial range of concentrations here.

IV. Conclusions

We have performed ab initio DFT calculations of interacting tetrasubstituted POSS molecules to help guide the development of a coarse-grained, or minimal, model of a tetratethered nanocube representing a POSS molecule with oligomeric substituents and subsequently employed this model in Brownian dynamics simulations to investigate tethered nanocube self-assembly. DFT calculations indicate that there is a weak, attractive interaction between two $cyhex_4$-substituted POSS molecules and very little distortion in the structures of the silsesquioxane cage upon molecular interaction. Calculations of the electron density distribution about the molecules show that the electron density is cubic in form. On the basis of these findings, we developed a minimal model of a tetratethered POSS molecule in

which the silesesquioxane cage is approximated as a rigid cube with eight beads constituting the cube vertices, and the polymer tethers are represented as bead−spring chains. We model the site−site attractive interactions between cubes using the simple Lennard-Jones 12−6 potential.

The minimal model was subsequently used in Brownian dynamics simulations to study the self-assembly of the tethered NBBs. The influence of solvent quality, temperature, and concentration on the resulting assemblies was obtained. We demonstrated that the thermodynamically driven immiscibility of tethers and nanocubes can be used to self-assemble tethered cubic NBBs into structures that are analogous to those observed in block copolymer and surfactant systems. In particular, the unique architecture of the tethered NBB studied here induces the molecules to self-assemble into hexagonally arranged cylindrical or columnar phases of cubic cross section and micelles in both neutral solvent and selective solvent that is good for the tether species and poor for the cube species. The nanocubes tend to pack face-to-face within a cylinder or micelle due to the geometry of the rigid cube. The flexibility of the tethers on the cube and the topology of the NBB appear to preclude a lamellar phase, thereby demonstrating a key difference between the self-assembly of tetratethered cubes and traditional surfactant and block copolymer systems. On the basis of simulation snapshots of configurations and the behavior of the pair interaction energies and the average tether mean-squared corner-to-end distance as a function of the Flory interaction energy parameter $\chi \sim \epsilon^* = \epsilon/k_BT$, we located the ODT phase boundaries and found that the transition from a disordered state to hexagonally arranged cylinders at high concentration appears to be discontinuous. At low concentration, systems of NBBs with short tether length $Nt = 2$ assemble into disordered spherical and elongated micelles. We found that systems of NBBs with longer tether length $Nt = 4$ decrease the concentration regime in which hexagonally arranged cylindrical phases form. The concentration regime in which spherical micelles form increased and the micelles ordered into a fcc-like pattern. We constructed semiquantitative phase diagrams for the tethered cubic NBBs and found them to share qualitative similarities with the phase diagrams for surfactant solutions, as well as differences that we attributed to the unique geometry and topology of the tetratethered NBB.

The simulations presented here utilize a simplified model to access the long length and time scales pertinent to the assembly process. Our minimal model captures the essential features of connectivity and interaction specificity for predicting self-assembled structures in a broad class of tethered NBB systems.[30] Here we have made a first attempt to simulate the self-assembly of tethered POSS molecules using simple interaction potentials based on insight gained from quantum mechanical calculations. Further refinement of the minimal model based on additional information obtained from quantum mechanical calculations, and atomistic simulations employing a highly accurate force field suitable for describing intermolecular interactions, is required to more faithfully capture the correct properties of these systems. Such a multiscale simulation framework is necessary for bridging the various length and time scales relevant to the assembly process. Further information obtained from accurate calculations at short length and time scales can be used to refine the parameters in our simple potentials, and thereby map our coarse-grained models to their atomistic counterparts, so that the appropriate molecular behavior is captured at longer length and time scales. Efforts in this direction are currently underway.

Acknowledgment. Financial support for this work has been provided by the National Science Foundation under Grant DMR-0103399. E.R.C. is grateful to A. S. Keys for valuable insights and discussions on analyzing the micellar systems and to M. H. Lamm, Z. L. Zhang, M. A. Horsch, and R. G. Larson for fruitful discussions. We thank E. B. Coughlin, R. M. Laine, and P. T. Mather for insightful conversations and P. T. Cummings, J. Kieffer, and C. McCabe for collaboration as part of a larger effort to model POSS−polymer systems. We also thank the National Partnership for Advanced Computational Infrastructure (NPACI) and the University of Michigan Center for Advanced Computing for computer cluster support.

Supporting Information Available: The configurations of interacting cyhex$_4$-POSS in the DFT calculations. This material is available free of charge via the Internet at http://pubs.acs.org.

References and Notes

(1) Whitesides, G. M.; Boncheva, M. *Proc. Natl. Acad. Sci. U.S.A.* **2002**, *99*, 4769−4774.
(2) Lichtenhan, J. D. *Comments Inorg. Chem.* **1995**, *17*, 115−130.
(3) Provatas, A.; Matisons, J. G. *Trends Polym. Sci.* **1997**, *5*, 327−332.
(4) Laine, R. M.; Zhang, C. X.; Sellinger, A.; Viculis, L. *Appl. Organomet. Chem.* **1998**, *12*, 715−723.
(5) Sanchez, C.; Soler-Illia, G.; Ribot, F.; Lalot, T.; Mayer, C. R.; Cabuil, V. *Chem. Mater.* **2001**, *13*, 3061−3083.
(6) Lichtenhan, J. D.; Schwab, J. J.; Reinerth, W. A. *Chem. Innov.* **2001**, *31*, 3−5.
(7) Feher, F. J.; Budzichowski, T. A. *Polyhedron* **1995**, *14*, 3239−3253.
(8) Li, G. Z.; Wang, L. C.; Ni, H. L.; Pittman, C. U. *J. Inorg. Organomet. Polym.* **2001**, *11*, 123−154.
(9) Pyun, J.; Matyjaszewski, K.; Kowalewski, T.; Savin, D.; Patterson, G.; Kickelbick, G.; Huesing, N. *J. Am. Chem. Soc.* **2001**, *123*, 9445−9446.
(10) Shockey, E. G.; Bolf, A. G.; Jones, P. F.; Schwab, J. J.; Chaffee, K. P.; Haddad, T. S.; Lichtenhan, J. D. *Appl. Organomet. Chem.* **1999**, *13*, 311−327.
(11) Zhang, C. X.; Bunning, T. J.; Laine, R. M. *Chem. Mater.* **2001**, *13*, 3653−3662.
(12) Saez, I. M.; Goodby, J. W. *J. Mater. Chem.* **2001**, *11*, 2845−2851.
(13) Saez, I. M.; Goodby, J. W.; Richardson, R. M. *Chem.−Eur. J.* **2001**, *7*, 2758−2764.
(14) Kim, K. M.; Chujo, Y. *Polym. Bull. (Berlin)* **2001**, *46*, 15−21.
(15) Feher, F. J.; Wyndham, K. D.; Scialdone, M. A.; Hamuro, Y. *Chem. Commun.* **1998**, 1469−1470.
(16) Feher, F. J.; Wyndham, K. D.; Knauer, D. J. *Chem. Commun.* **1998**, 2393−2394.
(17) Tamaki, R.; Tanaka, Y.; Asuncion, M. Z.; Choi, J. W.; Laine, R. M. *J. Am. Chem. Soc.* **2001**, *123*, 12416−12417.
(18) Abbenhuis, H. C. L. *Chem.−Eur. J.* **2000**, *6*, 25−32.
(19) Jeon, H. G.; Mather, P. T.; Haddad, T. S. *Polym. Int.* **2000**, *49*, 453−457.
(20) Mather, P. T.; Jeon, H. G.; Romo-Uribe, A.; Haddad, T. S.; Lichtenhan, J. D. *Macromolecules* **1999**, *32*, 1194−1203.
(21) Zheng, L.; Waddon, A. J.; Farris, R. J.; Coughlin, E. B. *Macromolecules* **2002**, *35*, 2375−2379.
(22) Pyun, J.; Matyjaszewski, K.; Wu, J.; Kim, G. M.; Chun, S. B.; Mather, P. T. *Polymer* **2003**, *44*, 2739−2750.
(23) Fu, B. X.; Lee, A.; Haddad, T. S. *Macromolecules* **2004**, *37*, 5211−5218.
(24) Knischka, R.; Dietsche, F.; Hanselmann, R.; Frey, H.; Mülhaupt, R.; Lutz, P. J. *Langmuir* **1999**, *15*, 4752−4756.

(25) Kim, K. M.; Keum, D. K.; Chujo, Y. *Macromolecules* **2003**, *36*, 867−875.
(26) Kim, B. S.; Mather, P. T. *Macromolecules* **2002**, *35*, 8378−8384.
(27) Cardoen, G.; Coughlin, E. B. *Macromolecules* **2004**, *37*, 5123−5126.
(28) Bharadwaj, R. K.; Berry, R. J.; Farmer, B. L. *Polymer* **2000**, *41*, 7209−7221.
(29) Lamm, M. H.; Chen, T.; Glotzer, S. C. *Nano Lett.* **2003**, *3*, 989−994.
(30) Zhang, Z. L.; Horsch, M. A.; Lamm, M. H.; Glotzer, S. C. *Nano Lett.* **2003**, *3*, 1341−1346.
(31) Ahmadi, T. S.; Wang, Z. L.; Green, T. C.; Henglein, A.; El-Sayed, M. A. *Science* **1996**, *272*, 1924−1926.
(32) Sun, Y. G.; Xia, Y. N. *Science* **2002**, *298*, 2176−2179.
(33) John, B. S.; Stroock, A.; Escobedo, F. A. *J. Chem. Phys.* **2004**, *120*, 9383−9389.
(34) Zhang, X.; Chan, E. R.; Glotzer, S. C. To be submitted for publication.
(35) Marcolli, C.; Calzaferri, G. *Appl. Organomet. Chem.* **1999**, *13*, 213−226.
(36) Sellinger, A.; Laine, R. M.; Chu, V.; Viney, C. *J. Polym. Sci., Part A: Polym. Chem.* **1994**, *32*, 3069−3089.
(37) Li, H.-C.; McCabe, C.; Striolo, A.; Cummings, P. T.; Lee, C.-Y.; Neurock, M. To be submitted for publication.
(38) Bieniok, A. M.; Bürgi, H. B. *J. Phys. Chem.* **1994**, *98*, 10735−10741.
(39) Kresse, G.; Furthmüller, J. *Phys. Rev. B* **1996**, *54*, 11169−11186.
(40) Vanderbilt, D. *Phys. Rev. B* **1990**, *41*, 7892−7895.
(41) Hammer, B.; Hansen, L. B.; Norskov, J. K. *Phys. Rev. B* **1999**, *59*, 7413−7421.
(42) Calzaferri, G.; Imhof, R.; Törnroos, K. W. *J. Chem. Soc., Dalton Trans.* **1994**, 3123−3128.
(43) Auf der Heyde, T. P. E.; Bürgi, H. B.; Bürgy, H.; Törnroos, K. W. *Chimia* **1991**, *45*, 38−40.
(44) Delley, B. *Comput. Mater. Sci.* **2000**, *17*, 122−126.
(45) Tsuzuki, S.; Lüthi, H. P. *J. Chem. Phys.* **2001**, *114*, 3949−3957.
(46) McCabe, C.; Glotzer, S. C.; Kieffer, J.; Neurock, M.; Cummings, P. T. *J. Comput. Theor. Nanosci.* **2004**, *1*, 265−279.
(47) Grest, G. S.; Kremer, K. *Phys. Rev. A* **1986**, *33*, 3628−3631.
(48) Kim, S. H.; Jo, W. H. *Macromolecules* **2001**, *34*, 7210−7218.
(49) Ding, J.; Carver, T. J.; Windle, A. H. *Comput. Theor. Polym. Sci.* **2001**, *11*, 483−490.
(50) Kim, K. H.; Kim, S. H.; Huh, J.; Jo, W. H. *J. Chem. Phys.* **2003**, *119*, 5705−5710.
(51) von Gottberg, F. K.; Smith, K. A.; Hatton, T. A. *J. Chem. Phys.* **1997**, *106*, 9850−9857.
(52) Allen, M. P.; Tildesley, D. J. *Computer Simulation of Liquids*; Clarendon Press: Oxford, 1987.
(53) Weeks, J. D.; Chandler, D.; Andersen, H. C. *J. Chem. Phys.* **1971**, *54*, 5237−5247.
(54) van Gunsteren, W. F.; Berendsen, H. J. C.; Rullmann, J. A. C. *Mol. Phys.* **1981**, *44*, 69−95.
(55) Grest, G. S.; Lacasse, M. D.; Kremer, K.; Gupta, A. M. *J. Chem. Phys.* **1996**, *105*, 10583−10594.
(56) Kubo, R. *Rep. Prog. Phys.* **1966**, *29*, 255−284.
(57) Larson, R. G. *J. Chem. Phys.* **1992**, *96*, 7904−7918.
(58) Guo, H.; Kremer, K. *J. Chem. Phys.* **2003**, *119*, 9308−9320.
(59) Stoddard, S. D. *J. Comput. Phys.* **1978**, *27*, 291−293.
(60) Rudnick, J.; Gaspari, G. *Science* **1987**, *237*, 384−389.
(61) Mackie, A. D.; Panagiotopoulos, A. Z.; Szleifer, I. *Langmuir* **1997**, *13*, 5022−5031.
(62) Lísal, M.; Hall, C. K.; Gubbins, K. E.; Panagiotopoulos, A. Z. *J. Chem. Phys.* **2002**, *116*, 1171−1184.
(63) Kenward, M.; Whitmore, M. D. *J. Chem. Phys.* **2002**, *116*, 3455−3470.
(64) Khalatur, P. G.; Khokhlov, A. R.; Nyrkova, I. A.; Semenov, A. N. *Macromol. Theory Simul.* **1996**, *5*, 713−747.
(65) Vasilevskaya, V. V.; Klochkov, A. A.; Lazutin, A. A.; Khalatur, P. G.; Khokhlov, A. R. *Macromolecules* **2004**, *37*, 5444−5460.
(66) McConnell, G. A.; Gast, A. P.; Huang, J. S.; Smith, S. D. *Phys. Rev. Lett.* **1993**, *71*, 2102−2105.
(67) Larson, R. G. *J. Phys. II* **1996**, *6*, 1441−1463.

MA047722L